DNS OF EGR-TYPE COMBUSTION IN MILD CONDITION

Y. Minamoto, T. D. Dunstan and N. Swaminathan

ym270@cam.ac.uk

Department of Engineering, University of Cambridge, Cambridge CB2 1PZ, United Kingdom

Abstract

Two-dimensional direct numerical simulations (DNS) of exhaust gas recirculation (EGR)-type combustion operated in moderate and intense low-oxygen dilution (Mild) combustion condition have been carried out to study the flame structure and its physics. The chemical reaction is modelled using a reduced two-step mechanism for hydrocarbon-air combustion. Simulated flame is then investigated from several aspects to study the effect of dilution on the structure of this flame front. The results suggest that the flame can be modelled with flamelet approaches, although the contribution of flame-flame interaction to mean reaction rate should be included quantitatively for accurate modelling of Mild combustion.

Introduction

The reduction of pollutant emissions and the increase of combustion efficiency are the key issues in the design and operation of engineering combustors such as GT engines. Exhaust gas recirculation (EGR) is a well-known method employed in automotive engines to avoid high oxygen concentration and to suppress $\mathrm{NO_x}$ emissions, since $\mathrm{NO_x}$ is formed when flame temperature and oxygen concentration are high. Extracting heat from the exhaust gases to preheat unburnt mixture is one way to improve thermal efficiency of the system.

Wünning and Wünning [1] presented a concept to achieve low formation of thermal NO even at high preheat temperature of mixture, which was then reviewed by Katsuki and Hasegawa [2], and Cavaliere and de Joannon [3]. This combustion is called flameless oxidation or moderate and intense low-oxygen dilution (Mild) combustion in which (1) air or reactant mixture is diluted with large amount of burnt mixture so that the maximum temperature rise is low in the combustor (2) air or fuel is significantly preheated, higher than the autoignition temperature for the given fuel. More specifically, if the inlet temperature of the reactant mixture, T_{in}, is higher than the mixture auto-ignition temperature, T_{ign}, and the maximum temperature increase, $\Delta T = T_{\mathrm{max}} - T_{\mathrm{in}}$, is lower than T_{ign}, the combustion condition is called Mild, where T_{max} is the maximum temperature. In conventional combustion, which is called feed-back combustion, $T_{\mathrm{ign}} > T_{\mathrm{in}}$ and $\Delta T > T_{\mathrm{ign}}$. If $T_{\mathrm{ign}} < T_{\mathrm{in}}$ and $\Delta T > T_{\mathrm{ign}}$, the combustion is classified as high temperature air combustion (HiTAC). These definitions can be shown clearly using a diagram as in Fig 1. The points marked denote the flame conditions studied here and will be discussed later. Therefore, temperature difference between unburnt and burnt mixture is relatively small in Mild combustion compared with conventional combustion and thus temperature variation is nearly homogeneous. This uniformity of temperature can also help to reduce combustion instabilities, which generally occurs when recirculation rates become high [1, 2].

Several studies have been carried out to further our understanding of Mild combustion [4–9]. Although a OH-PLIF [6] of Mild combustion zone showed a non-flamelet like structure, the simulations of Coelho and Peters [5] and Dally et al.[7] using flamelet models for non-premixed combustion showed a consistent trend with experimental measurements for a number of quantities. The OH-PLIF images for Mild combustion with premixed reactant reported by Özdemir and Peters [6] are insufficient to draw a conclusion on the structure of the reaction zones. Given the environmentally friendly nature of this combustion mode, it is useful to pose a question; what is the flame front structure in Mild combustion? We believe that finding an answer to this question would help to construct a modelling framework for Mild combustion.

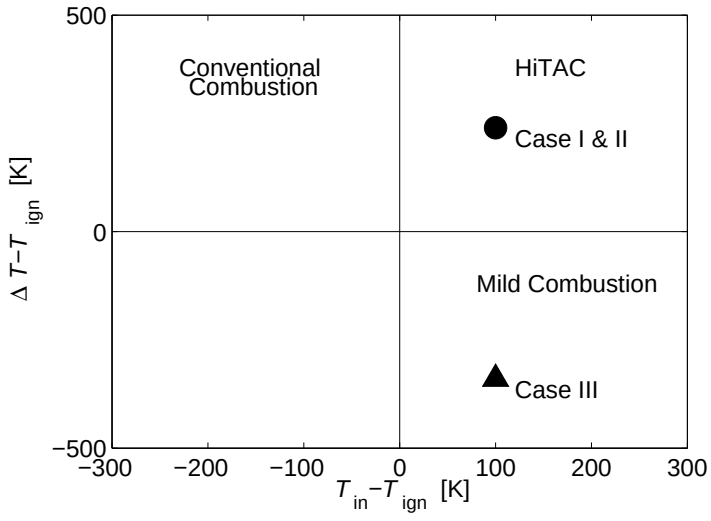

Figure 1. A classification of three flame conditions studied in the diagram [3].

Specifically, we like to ask whether flamelet assumptions are valid or whether the flame front is still flamelet like in Mild combustion conditions. Furthermore, combustion that takes place in EGR-type combustors is considered to be different from traditional turbulent flames; pockets of burnt gas and radicals, which are not well mixed before combustion, can lead to additional complexities such as flame-flame interaction. In such flame configurations together with Mild combustion conditions, flame structure is one of our interests and it has not been investigated yet in detail.

In this study, two-dimensional direct numerical simulation (DNS) is carried out for EGR-type combustion with a highly preheated and diluted methane-air mixture, as the preliminary step for three-dimensional DNS. The competing effects of radical and intermediates formation and their consumption are included in the simulation by using a systematically reduced two-step reaction for methane-air combustion. Mild combustion with premixed reactants are considered. Basic flame features are then investigated to study flame front structure in this mode of combustion.

Two-step mechanism

The chemical kinetics of methane-air combustion is modelled using a two-step reduced mechanism with non-unity Lewis numbers. This two-step mechanism involves six reactive species (+ N_2). The earlier two-step mechanism [10] is modified for lean premixed flame. This mechanism is:

$$\mathrm{CH_4 + O_2 \rightarrow H_2 + CO + H_2O}, \qquad \mathrm{(R1)}$$
$$\mathrm{O_2 + H_2 + CO \rightarrow H_2O + CO_2}, \qquad \mathrm{(R2)}$$

which includes the competition between two chemical time scale, R1 for the production of intermediate species and consumption of reactant, and R2 for consumption of intermediate species. The rates of these two reaction steps are:

$$\dot{\omega}_{R1} = 4.68 \times 10^{13} \exp\left(\frac{-7640}{T}\right) [\mathrm{CH_4}][\mathrm{R}], \qquad (\mathrm{mol/cc \cdot s}) \tag{1}$$

$$\dot{\omega}_{R2} = 5.34 \times 10^{16} T^{-1.8} [\mathrm{O_2}][\mathrm{R}]\mathcal{P}, \qquad (\mathrm{mol/cc \cdot s}) \tag{2}$$

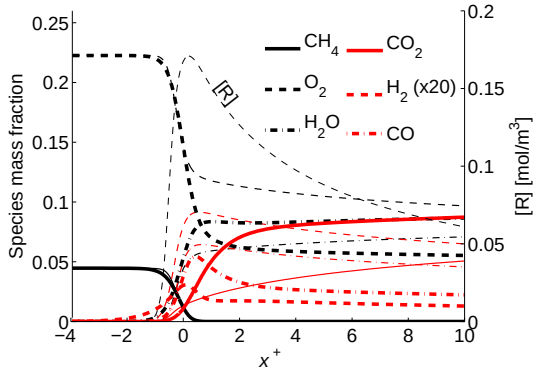

Figure 2. Laminar flame front structure simulated by two-step mechanism (thin lines) and GRI-3.0 mechanism (bold lines) for $\phi = 0.8$ and $T_u = 1200$ K.

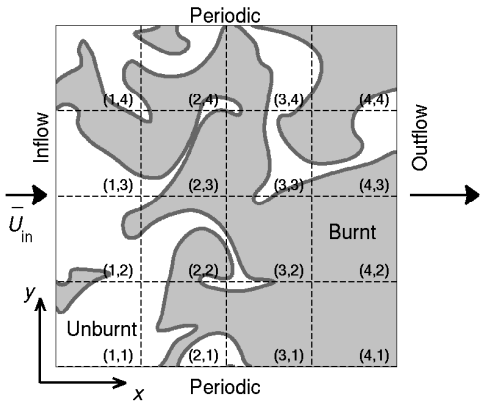

Figure 3. Schematic flame and numerical configurations, and divisional grids for post-processing of conditional averages.

where the radical concentration [R] is calculated as:

$$[\mathrm{R}] = \frac{2.7 \times 10^5 \exp(2300/\mathrm{T})}{\mathcal{P}} [\mathrm{O_2}]^{0.5} [\mathrm{H_2}]^{1.5} \exp\left(-\sqrt{15/4}\lambda' \frac{[\mathrm{CH_4}]}{[\mathrm{O_2}]}\right), \quad (\mathrm{mol/cc}) \tag{3}$$

where λ' is a parameter and it is related to the ratio of the rate of fuel consuming elementary reaction to chain branching reaction [10] and it is set to be 0.75. The thermodynamic pressure $\mathcal{P}$ is taken to be one atmosphere. The reaction R1 and R2 release about 40% and 60% of the overall heat release. The structure of a laminar premixed flames predicted by the above two-step mechanism and GRI-3.0 mechanism are shown in Fig. 2.

For this laminar and turbulent flames simulations, non-unity Lewis number is used and Prandtl number is set to be 0.7. The flame front structure is well captured by the two-step mechanism especially in preheat-reaction zones, although the mass fraction of products is underestimated in burnt zone. But this does not affect flame dynamics simulated in DNS, because the reactions occurs in this zone are mainly recombination reactions which have relatively slow chemical time-scale and the heat released by these reactions is not typically large. Several flame quantities, such as laminar flame speed, S_L, flame time-scale, τ_F, and burnt temperature, T_b, are also calculated with the two-step mechanism and agree reasonably with GRI-3.0 values for wide range of flame conditions relevant for Mild combustion ($T_u = 300 - 1200$ K, $\phi = 0.8$, $X_{\mathrm{O_2,u}} = 0.095 - 0.19$). The predicted flame speeds, for example, ranges 1.32-1.81 times the value given by GRI-3.0 mechanism. The flame time-scale is 1.23-1.90 of those predicted by GRI-3.0 mechanism. Ideally, a complex mechanism can be used for more accurate prediction, but its use requires significantly large computational resources. It should be noted that the stiffness problem can also be circumvented by using the two-step mechanism.

Configuration and numerical implementation

The numerical code used in this study is SENGA2, an updated version of SENGA [11]. Compressible transport equations are solved on a uniform grid for mass, momentum, total internal energy, and the mass fractions of N chemical species using the temperature dependent transport properties. Here, $N = 7$ for the two-step mechanism described above. Spatial derivatives are obtained using a tenth order central difference scheme which gradually reduces to fourth

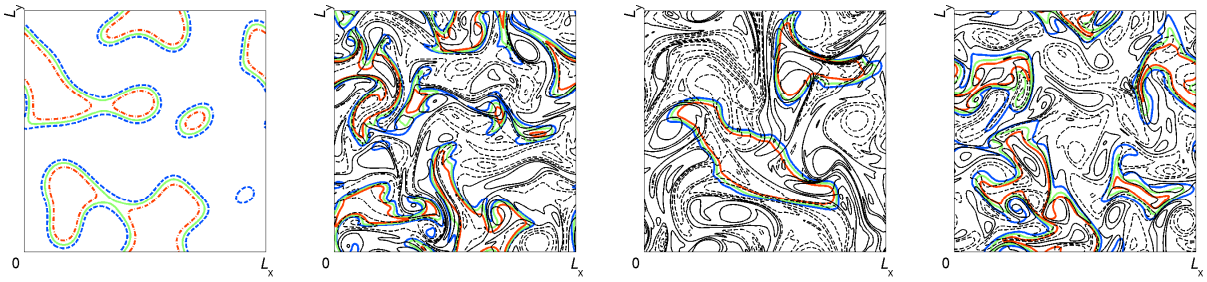

Figure 4. Scalar and turbulence fields obtained each stage of preprocessing. (a) c-field obtained in step (ii). Blue lines: $c = 0.2$, green lines: 0.5, and red lines: 0.8, and fields obtained at step (iii) for (b) case I, (c) case II, and (d) case III. Solid-black lines: positive vorticity, dashed-lines: negative vorticity,

order central difference scheme near boundaries and then is replaced by a fourth order one-sided differencing on boundaries. Time integration is performed using third order Runge-Kutta scheme.

Figure 3 shows the numerical configuration and its coordinate. The domain is square with non-reflecting outflow boundary on the downstream (x-direction) and periodic in the y-direction. A mixture of exhaust gas and fresh premixed gas is fed from the left boundary at an average velocity of $\bar{U}_{in}$. Navier-Stokes characteristic boundary conditions (NSCBC) [12] are applied to non-reflecting outflow boundary. In general, flow is locally assumed as one-dimensional and inviscid (LODI) on the boundary and all incoming characteristic wave amplitude variations from target value are estimated by neglecting transverse convective, diffusive and source terms. However, in present case, flow and scalar fields have gradient on the boundary in both normal and transverse directions to the boundary and also flame-boundary interaction is inevitable. Therefore, additional contribution due to transverse convective, diffusive and source terms are taken into account to estimate the amplitude variation of incoming pressure wave [13–16].

Preprocessing of scalar and velocity fields for inflow and initial conditions

The mixture used in this DNS is in the state of partially premixed between fresh reactant and exhaust gas, which is assumed as the inlet gases for the EGR-type combustion. The steps described below are followed to achieve the desired fields: (i) The turbulence field is generated in a preliminary DNS of freely decaying, homogeneous isotropic turbulence in a periodic domain. Initial turbulence for this run is generated as in [17], and the simulation is continued until turbulence is fully developed. (ii) A homogeneous scalar field is obtained using the method in [18] and this field is taken to be progress variable field varying from 0 to 1. The region with $c = 0$ is taken to have unburnt reactants and the products at temperature T_b' consists in region with $c = 1$. The mass fraction and density fields obtained from unstrained laminar flame simulation calculated with the two-step chemistry using SENGA2 for the reactant mixture of interest are used to construct the scalar fields. (iii) These fields are then allowed to evolve in a periodic domain to mimic the EGR-mixing before they are used for reacting simulation. Temperature is also allowed to evolve during this simulation resulting in a temperature fluctuation less than 5 %. Figure 4a shows the c-field obtained in procedure (ii) above which does not have any correlation with velocity field. Figures 4b-4d are the results of procedure (iii). These turbulence and scalar fields are used as the initial condition and the inlet mixture fields in combustion DNS.

Since both velocity and scalar to be fed for combustion DNS are fixed at the inlet boundary

Table 1. Flame and turbulence parameters

Case	X_{O_2}	u'/S_L	$\bar{U_{in}}/S_L$	l_0/δ_F	l_0/δ_{th}	Re_{l_0}	Da	Ka	l_0/l_c	τ_D/τ_F
I	0.194	2.62	10.1	33.7	1.75	126.1	12.9	0.73	1.50	1.67
II	0.194	5.71	10.1	50.2	2.61	410.1	8.79	1.93	1.21	1.67
III	0.095	2.38	8.70	20.9	1.12	71.05	8.79	0.80	1.15	1.70

by the pre-simulation after the step (iii) above, nearly the same flame appears for every flow-through time, τ_D, which is the mean convection time from the inlet to outlet boundaries, during combustion DNS. In order to avoid this, a small fluctuation, y_i', is added to the mass fraction field at inlet using

$$Y_i(x=0,y,t) = \hat{Y}_i(\underline{x}(t),y) + \alpha(t) y_i'(\underline{x}(t),y). \tag{4}$$

Here, $\hat{Y}_i$ corresponds to the scalar field obtained after procedure (iii) as in Figs. 4(b)-4(d). $\underline{x}(t)$ is the $x-$ location of scanning plane at time, t, moving at $\bar{U}_{in}$ inside the pre-simulation domain. The fluctuation, y_i', is constructed in the same method used in procedure (ii) for c field with a modification so that; (a) the spacial average of y_i' in the entire field is zero for each species, and (b) the value of y_i' is within $\pm 0.25 Y_{i,\max}$. Note that there is no correlation between $\hat{Y}_i(y,t)$ field and $y_i'(y,t)$ field, but the length scales of y' is chosen to be comparable to those of $\hat{Y}_i$. The factor, $\alpha(t)$, is specified as $\alpha = \sin[\omega_D(t-t_0)]$ for $t \geq t_0$ and $\alpha = 0$ for $t < t_0$, where ω_D and t_0 are set to be $\pi/(2\tau_D)$, and $2\tau_D$, respectively. Therefore, this fluctuation is included into the domain from $t = t_0$, until $t = t_0 + 4\tau_D$ so that the average of $\alpha y_i'$ is close to zero over the period of $4\tau_D$.

Computational parameters and conditions

Three cases are simulated with different turbulence levels and length scale ratio between scalar and turbulence fields. Equivalence ratio, ϕ, is fixed to be 0.8 for all cases. The inlet and initial temperatures are set as $T_b' \approx 1200\mathrm{K}$ for all cases. The turbulence and flame quantities for case I-III are given in Table 1. The molar fraction of oxygen, X_{O_2}, in the unburnt gas indicates the dilution levels. For case I and II, the mixture comprises of undiluted reactants ($\phi = 0.8$) and its burnt gas. For case III, the unburnt mixture is diluted 50% (by mass base) using $\mathrm{H_2O}$ and $\mathrm{CO_2}$, and then it is mixed with its burnt gas. The auto-ignition temperature for the mixture used in this study is about 1100 K. The maximum temperature difference ($\Delta T = T_{\mathrm{WSR}} - T_u$) during combustion is about 1340 K for the undiluted mixture ($X_{\mathrm{O}_2} = 0.194, \phi = 0.8$) and 760 K for the diluted mixture ($X_{\mathrm{O}_2} = 0.095, \phi = 0.8$), where T_{WSR} is the working temperature of a well-stirred reactor (WSR) computed using the commercial software Cosilab with a residence time of 1 s [3]. Thus the flame conditions in case I and II are in the high temperature combustion condition and flame III is the Mild combustion region as in Fig 1.

Thermal thickness, δ_{th} is defined as $(T_b - T_u)/|\nabla T|_{\max}$, and δ_F is Zeldovich thickness defined as $\delta_F = D/S_L$, where T_u, T_b and D denote unburnt gas temperature, burnt gas temperature and the mass diffusivity respectively. For flames I and II, $\delta_{th} = 0.594\mathrm{mm}$ and for flame III, $\delta_{th} = 1.35\mathrm{mm}$. The turbulent Reynolds number, Re_{l_0}, based on the integral length scale of initial and inlet turbulence, l_0, and its rms velocity, u', shows case II has the strongest and case III has the weakest turbulence. The Damköhler number, Da, is define as the ratio between eddy turn over time (l_0/u') to flame time (δ_F/S_L), and cases II and III have similar values. For reference, if one would like to use the Damköhler defined as $(l_0/\delta_{th})/(u'/S_L)$ as is often used [19], it rages between 0.46 and 0.67 for the cases in Table 1. The Karlovitz number is calculated as $Ka \approx (u'/S_L)^{3/2}(l_0/\delta_F)^{-1/2}$. These conditions are classified as corrugated flamelets (case

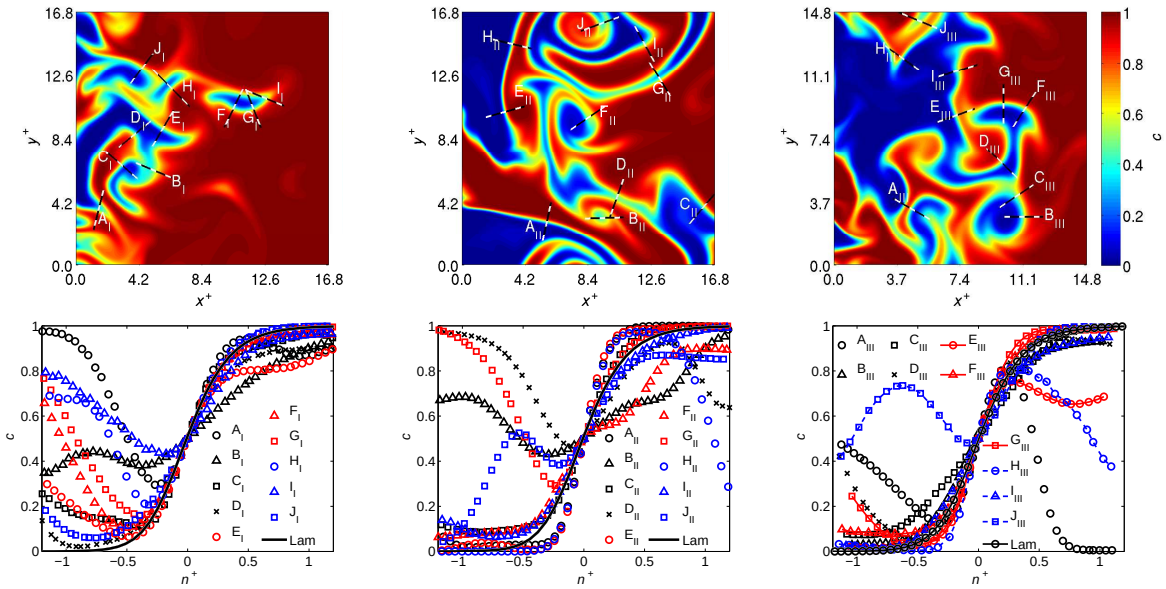

(a) Case I **(b)** Case II **(c)** Case III

Figure 5. Instantaneous progress variable fields at $t = 1.7\tau_D$ in the top row. Black and white dashed lines are locations for which the variation of c along the normalized flame normal distance is shown in the bottom row. The planar laminar premixed flame solution for the corresponding mixture is also shown.

I and III) and thin reaction zones (case II), although all conditions are close to the border between these two conditions if one may use the classical regime diagram for turbulent premixed combustion [20]. The ratio of integral length scale of turbulence and scalar, l_c, is comparable for all the cases. This scalar length scale is calculated using the mass fraction of $\mathrm{CH_4}$.

640×640 grid points are used for all the cases. The domain sizes are $L_x \times L_y = 10\mathrm{mm} \times 10\mathrm{mm}$ for cases I and II, and $20\mathrm{mm} \times 20\mathrm{mm}$ for case III. These sizes respectively correspond to $16.8\delta_{th}$ and $14.8\delta_{th}$.

Results and discussions

Since the flame structure in the progress variable space is independent from flame configuration, the progress variable is used to study flame front and its inner structure. Here, the progress variable is defined from the mass fraction of $\mathrm{CH_4}$ as $c = 1 - Y_{\mathrm{CH_4}}/Y_{\mathrm{CH_4,u}}$. Although, non-unity Lewis number is used in present DNS, it is expected that the definition of the progress variable will not unduly influence the insight obtained in this study. All instantaneous/mean results used here are obtained in the period from τ_D to $6\tau_D$ from the initialization to ensure that the effects of initialization have disappeared.

The instantaneous progress variable fields are shown for cases I-III in the top row of Fig. 5(a) to (c), where the domain lengths are normalized using δ_{th} . The spatial variation of c is quite different from the conventional turbulent planar flames and the presence of unburnt pocket and flame interactions of various kind is obvious in Fig. 5. The spatial extent of interaction events is increased when u'/S_L is increased as shown in Fig 5b for case II. The size of unburnt pocket seem to scale with the normalized turbulence length scale, l_0/δ_{th}. The main interest here is to study if the flame front has flamelet characteristics when the mixture is highly diluted and preheated, and the flame front interacts with one another.

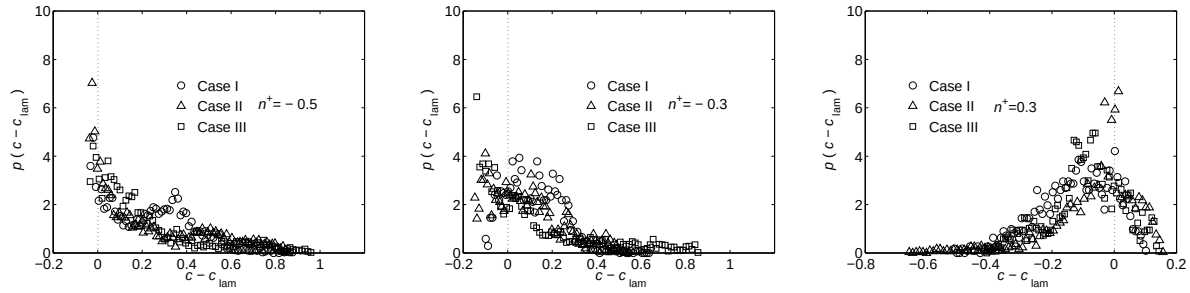

(a) $n^+ = -0.5$ **(b)** $n^+ = -0.3$ **(c)** $n^+ = 0.3$

Figure 6. Probability density function of the deviation of progress variable from the laminar flame value at the same normalized flame normal distance, (a): $n^+ = -0.5$, (b) $n^+ = -0.3$, and (c): $n^+ = 0.3$. Plots are taken from $t = 1.7\tau_D$ instantaneous result.

Several locations are arbitrarily selected, the black and white dashed lines in Fig. 5, to study the variation of the progress variable as a function of the flame normal distance, n^+. These variations are shown in the bottom row of Fig. 5. The result of 1D planar laminar flame is also shown for comparison. The location for $n^+ = 0$ corresponds to $c = 0.5$ and generally increases towards product side, although this is not always the case, since there is flame interaction. The effect of flame interaction on the flame front structure is apparent in Fig. 5 as the deviation from 1D laminar flame result for $n^+ < 0$. However, the variation of the progress variable in non-interacting flame, such as $\mathrm{C_I}$, $\mathrm{D_I}$, $\mathrm{J_I}$, $\mathrm{A_{II}}$, $\mathrm{C_{II}}$, $\mathrm{E_{II}}$, $\mathrm{G_{II}}$, $\mathrm{I_{II}}$, $\mathrm{B_{III}}$, $\mathrm{D_{III}}$, $\mathrm{F_{III}}$ and $\mathrm{I_{III}}$ is quite close to laminar flame structure. For other interacting regions, such as $\mathrm{A_I}$, $\mathrm{E_I}$, $\mathrm{F_I}$, $\mathrm{G_I}$, $\mathrm{H_I}$, $\mathrm{I_I}$, $\mathrm{D_{II}}$, $\mathrm{G_{II}}$, $\mathrm{J_{II}}$, $\mathrm{A_{III}}$, $\mathrm{E_{III}}$, $\mathrm{H_{III}}$ and $\mathrm{J_{III}}$, flame is partially flamelet-like. If one takes a close look at $\mathrm{D_{II}}$ and G_{II} in Fig. 5, it seems that flames keep flamelet shape even during interaction until their flame fronts completely collide and disappear. However, $\mathrm{B_I}$ and $\mathrm{B_{II}}$ show that there are local flames which might not be flamelet like. Probability density function of deviation of instantaneous c from the laminar flame value, c_{lam}, for a given n^+ is shown in Fig. 6. The pdf shows high value around $c - c_{\mathrm{lam}} = 0$, especially at $n^+ = -0.5$ and 0.3. Plots of high probability are distributed relatively wide in $n^+ = -0.3$ (Fig. 6b) and this is because of the effect of flame interaction on the flame front as shown in Fig 5.

Figures 7(a) and (b) show variations of species mass fraction for cases II and III for four sample locations from Fig. 5. The variations of mass fractions in the laminar flame are also shown for comparison. These variations reflect the $c - n^+$ plots: for $\mathrm{C_{II}}$ and $\mathrm{B_{III}}$ cross-sections, which have a quite similar c variation to laminar flame, also have close variations of mass fractions as in the laminar flames. For $\mathrm{J_{II}}$ and $\mathrm{J_{III}}$, mass fraction variations deviate at the same location where the progress variable variation deviates from the laminar flame case. Where the progress variable is higher than the laminar flame value for location $\mathrm{J_{II}}$, specifically for $-1 \leq n^+ \leq -0.2$ due to the flame interaction, consumptions of reactant and oxidizer are found to be high for these locations. The mass fractions variation at cross-section $\mathrm{J_{III}}$ shown in Fig. 7(b) have similar behaviour if one compares Figs. 5(c) and 7(b). These behaviours are also found to be typical for case I (not shown) as well. The effects of dilution do not seem to alter the flame front structure from the planar laminar case for the conditions investigated in this study.

The conditional average of mass fractions based on the progress variable, $Q_i(\zeta; x, y) = < Y_i | c = \zeta, x, y >$, is shown in Figs 7(c) and (d). The average is taken in time and within the divisional grid space shown in Fig. 3. The thin lines are the DNS results and the bold lines are the laminar flame values. Both figures show that the conditional mass fractions have

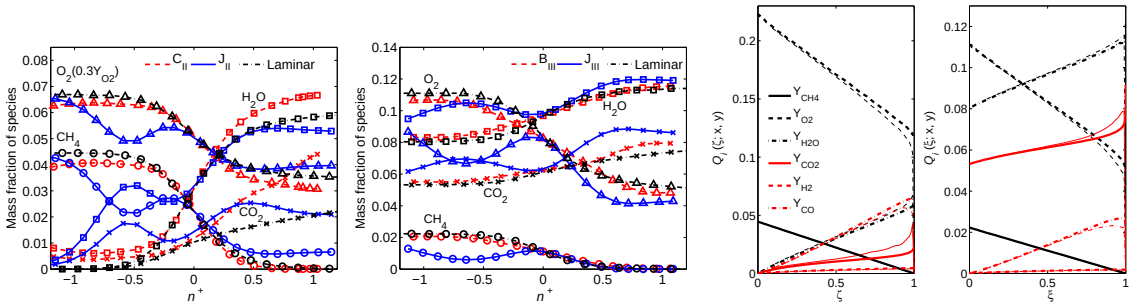

(a) Case II **(b)** Case III **(c)** Case II, (3,3) **(d)** Case III, (4,2)

Figure 7. (a) and (b): Instantaneous variation of species mass fraction vs normalized flame normal distance along the cross-section shown in Figs. 5(b) and (c) for cases II and III. (c) and (d): Conditional average of species mass fraction based on progress variable at sub-grid (3,3) for (c) and (4,2) for (d) as in Fig. 3.

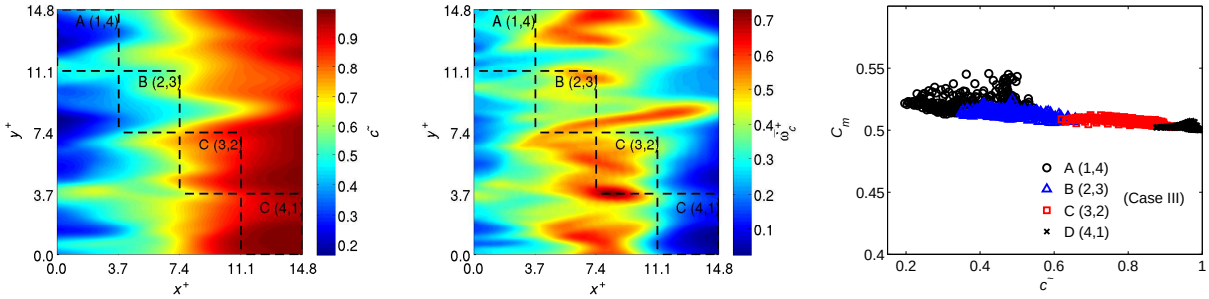

(a) $\tilde{c}$ **(b)** $\dot{\bar{\omega}}_c^+$ **(c)** $\tilde{c} - C_m$

Figure 8. (a): spatial variation of the progress variable and the normalized mean reaction rate, and locations of sampling region for case III. (b): Scatter plot of the progress variable vs the model constant, C_m, at each sampling region (case III).

similar variation to laminar flame and the effect of flame interaction or oxygen dilution does not seem to affect the conditional values. These results are typical even for other locations in all the cases. For the both cases shown in Fig. 7, the mass fraction of products (H_2O and CO_2) are slightly higher than the laminar flame values, especially for $0.6 \leq \zeta \leq 1.0$. This is considered as the contribution of the recombination process of reactions which takes place in burnt side, since, there can be burnt pocket at the inlet and at such a pocket has enough resident time to generate products by using up radicals. However, the difference from laminar flame case due to this contribution is small, and it is clear that the flames simulated here have flamelet-like behaviour. Although, these plots are also averaged in a sub-grid space shown in Fig. 3, it is believed that $Q_i(\zeta; x, y)$ will have similar variation if one uses enough realizations to construct the conditional average as per Reynolds Averaged Navier Stokes (RANS) modelling framework.

It is also useful to see the correlation between the mean reaction rate, $\bar{\dot{\omega}}_c$, and the mean scalar dissipation rate, $\tilde{\epsilon}_c$, since their direct relation is written as [21, 22]

$$\bar{\dot{\omega}}_c = 2/(2C_m - 1)\bar{\rho}\tilde{\epsilon}_c. \tag{5}$$

The C_m is the model parameter and its typical value is 0.7-0.8 for lean hydrocarbon flames. This relation is strictly valid for purely premixed, unity Lewis number flames when the flame front thickness is smaller than Kolmogorov length scale. Figure 8 (a) and (b) show the mean progress variable and the mean reaction rate, $\bar{\dot{\omega}}_c$, for case III. The mean reaction rate is normalized using ρ_u, S_L and δ_{th}. In Figs. 8(a) and (b), the spatial variations of the mean progress variable and the normalized mean reaction rate show that intense reaction takes place in middle portion of the computational domain, although mean reaction rate is non-zero near the boundaries unlike in the planar flames. This is due to the flame configuration where reaction can take place anywhere in the domain unlike conventional planar turbulent flame where flame front locates in the center of domain in average. In other cases, the spatial distribution of mean reaction rate is similar, although the shape of high reaction rate area varies from case to case, since they are controlled by the scalar and turbulence field fed from the inlet boundary. Figure 8 (c) shows scatter plot of the $\tilde{c} - C_m$ relations sampled from the four sampling regions shown as A, B, C, and D in Fig. 8(a) and (b). The plots show only one in every 100 points. The results clearly show that C_m is close to a constant value from 0.5 to 0.55.

Summary
Two-dimensional DNS of EGR-type combustion has been carried out with partially premixed methane-air mixture using a two-step mechanism. The mixture is highly preheated and diluted/undiluted which corresponds to Mild/HiTAC condition. The simulated flames are then analysed to study its flame front structure. The instantaneous and averaged data show that the simulated flames have flamelet-like behaviour although the effect of flame interaction can be observed. Three-dimensional DNS of similar flame configuration will be conducted for further investigations and modelling purposes.

Acknowledgements
YM acknowledges the financial support of Nippon Keidanren. The support of EPSRC by grant EP/F028741/1 is acknowledged by TDD and NS.

References

[1] Wünning, J. A. and Wünning, J. G., Flameless oxidation to reduce thermal NO-formation. *Prog. Energy Combust. Sci.*, 23, 81–94 (1997).
[2] Katsuki, M. and Hasegawa, T., The science and technology of combustion in highly preheated air. pp. 3135–3146 (1998).
[3] Cavaliere, A. and de Joannon, M., Mild combustion. *Prog. Energy Combust. Sci.*, 30, 329–366 (2004).
[4] de Joannon, M., Saponaro, A., and Cavaliere, A., Zero-dimensional analysis of diluted oxidation of methane in rich conditions. *Proc. Combust. Inst.*, 28, 1639–1646 (2000).
[5] Coelho, P. J. and Peters, N., Numerical simulation of a mild combustion burner. *Combust. Flame*, 124, 503–518 (2001).
[6] Özdemir, I. B. and Peters, N., Characteristics of the reaction zone in a combustor operating at mild combustion. *Exp. Fluids*, 30, 683–695 (2001).
[7] Dally, B. B., Riesmeier, E., and Peters, N., Effect of fuel mixture on moderate and intense low oxygen dilution combustion. *Combust. Flame*, 137, 418–431 (2004).
[8] Galleti, C., Parente, A., and Tognotti, L., Numerical and experimental investigation of a mild combustor burner. *Combust. Flame*, 151, 649–664 (2007).
[9] Kobayashi, H., Yata, S., Ichikawa, Y., and Ogami, Y., Dilution effects of superheated water vapor on turbulent premixed flames at high pressure and high temperature. *Proc. Combust. Inst.*, 32, 2607–2614 (2009).

[10] Swaminathan, N. and Bilger, R. W., Direct numerical simulation of turbulent nonpremixed hydrocarbon reaction zones using a two-step mechanism. *Comb. Sci. Technol.*, 127, 167–196 (1997).
[11] Cant, R. S., Direct numerical simulation of premixed turbulent flames. *Phil. Trans. R. Soc. Lond. A.*, 357, 3583–3604 (1999).
[12] Poinsot, T. and Lele, S., Boundary conditions for direct simulations of compressible viscos flows. *J. Comput. Phys.*, 101, 104–129 (1992).
[13] Sutherland, J. C. and Kennedy, C. A., Improved boundary conditions for viscous, reacting, compressible flows. *J. Comput. Phys.*, 191, 502–524 (2003).
[14] Prosser, R., Improved boundary conditions for the direct numerical simulation of turbulent subsonic flows. i. inviscid flows. *J. Comput. Phys.*, 207, 736–768 (2005).
[15] Yoo, C. S. and Im, H. G., Characteristic boundary conditions for simulations of compressible reacting flows with multi-dimensional, viscous reacting effects. *Combust. Theory Model.*, 11, 259–286 (2007).
[16] Dunstan, T. D., Swaminathan, N., Bray, K. N. C., and Cant, R. S., Geometrical propaties and turbulent flame speed measurements in stationary V-flames using direct numerical simulation. *Flow Turbulence Combust.* (2010).
[17] Rogallo, R. S., Numerical experiments in homogeneous turbulence. *NASA TM*, 81315 (1981).
[18] Eswaran, V. and Pope, S. B., Direct numerical simulations of the turbulent mixing of a passive scalar. *Phys. Fluids*, 31, 506–520 (1987).
[19] Hawkes, E. R. and Chen, J. H., Comparison of direct numerical simulation of lean premixed methane-air flames with strained laminar flame calculations. *Combust. Flame*, 144, 112–125 (2006).
[20] Peters, N., *Turbulent combustion*. Cambridge University Press (2000).
[21] Bray, K. N. C., The interaction between turbulence and combustion. *Proc. Combust. Inst.*, 17, 223–233 (1979).
[22] Libby, P. A. and Bray, K. N. C., Implications of the laminar flamelet model in premixed turbulent combustion. *Combust. Flame*, 39, 33–41 (1980).